J. Fluid Mech. (1990), *vol.* 215, *pp.* 571–583
Printed in Great Britain

Surface-tension-driven Bénard convection in small containers

By E. L. KOSCHMIEDER AND S. A. PRAHL
College of Engineering, The University of Texas at Austin, Austin, TX 78712, USA

(Received 12 May 1989)

The onset and the form of surface-tension-driven convection in three different small circular and one small square container has been studied experimentally. In the smallest circular container, with increasing aspect ratio, the pattern consisted of first a circular roll and then segments of a circle outlined by different numbers of azimuthal nodal lines, with up to six segments. Simple solutions in the square container were the one-cellular pattern and a pattern consisting of four square cells. Unexpected solutions formed when the number of the cells in the square container was not a square number. When the aspect ratio permitted two cells, two triangular cells were observed. With space for three cells, one square cell and two wedge-shaped cells formed. The onset of convection in all fluid layers was characterized by a steep increase of the critical Marangoni number with decreasing aspect ratio.

1. Introduction

As is well known, the cause of the formation of the hexagonal convection cells observed by Bénard (1900) is surface tension, or more accurately, the variation of the surface tension coefficient with temperature, as was established theoretically by Pearson (1958). The tendency to form hexagonal convection cells when the fluid layer is under an air surface and convection is caused by heating from below is so clearly apparent, that one can say that the hexagonal cell form is the unique solution of the pattern selection mechanism; even though many of the observed patterns are more polygonal than hexagonal, presumably because of imperfections of the supposedly uniform temperatures either beneath or above the fluid. One wonders whether the tendency to form hexagonal cells is still prevalent when geometric constraints by nearby walls in small containers make the hexagonal form less likely. We have, therefore, made a series of experiments trying to gain insight into the formation of the patterns, and the preference for the hexagonal cells. The onset and the form of surface-tension-driven Bénard convection in small circular and rectangular containers has been studied theoretically by Rosenblat, Davis & Homsy (1982) and by Rosenblat, Homsy & Davis (1982). They predict that in small circular containers motion will occur in cells whose boundaries are either circular concentric, or given by azimuthal nodal lines, so that the cells appear like pieces of pie. In rectangular containers they predict the appearance of roll type cells whose axes are aligned with the shorter dimension of the rectangular container, similar to the planform of convection in rectangular containers in Rayleigh–Bénard convection, which were studied by Davis (1967). Besides the form of the motion, Rosenblat *et al.* predict the values of the critical Marangoni number required for onset of convection, in the absence of buoyancy, i.e. in the case where the Rayleigh number is zero.

The Marangoni number is given by

$$Ma = \frac{\mathrm{d}S}{\mathrm{d}T}\frac{\Delta T d}{\rho \nu \kappa}, \tag{1}$$

and the Rayleigh number is given by

$$R = \frac{\alpha g \Delta T d^3}{\nu \kappa} \tag{2}$$

where $\mathrm{d}S/\mathrm{d}T$ is the variation of the surface tension coefficient with temperature, ΔT the temperature difference applied to the fluid, d the depth of the fluid, ρ the density of the fluid, α the volume expansion coefficient of the fluid, ν the viscosity and κ the thermal diffusivity of the fluid. Rosenblat *et al.* (1982*a*) predict a very sharp increase of the critical Marangoni number with decreasing aspect ratio of the fluid, just as in the corresponding Rayleigh–Bénard problem in rectangular containers (Davis 1967) and in circular containers (Charlson & Sani 1970). We will, in the following, discuss experiments which investigate the planform of the motion as well as the value of the critical Marangoni numbers for onset of surface-tension-driven convection in small circular containers, as well as in a square container.

2. Description of the apparatus

The apparatus is in essence the same apparatus as described in Koschmieder & Biggerstaff (1986), adapted to the work with small containers. Only the most important features can be discussed here, for a sketch of the original apparatus see Koschmieder & Biggerstaff. The bottom of the apparatus is a 5 cm thick copper block of 17.8 cm diameter which is heated electrically with a resistance wire. The top of the copper block should have a practically uniform temperature. On top of the copper block is a lucite frame with a circular inner opening of 13.55 cm diameter. Into this opening and on top of the copper block we placed a bakelite plate of 8 mm thickness, into which three circular holes of different diameter and one square hole were cut. These holes received the small containers with which the experiments were made. The bakelite plate served as thermal insulation in the horizontal direction from one container to the others. The bakelite plate was covered with a glass plate of 2.32 mm thickness. The glass plate was cooled by circulating water, and was, for all practical purposes, of uniform temperature, and fixed the temperature of the air on top of the fluid in the small containers.

The bases of the four small fluid containers were made of brass, and were of the same thickness, so that the bottom temperatures of the fluid in the containers were all the same. The surfaces of the brass bases were polished to a mirror finish. The circular bases were of 12.7 mm, 19.05 mm and 25.4 mm diameter; the sides of the square container were 12.7 mm long. The oil on top of the brass bases was confined laterally by lucite walls of 0.75 mm thickness in the case of the circular containers, and by a 1 mm thick seamless piece of square lucite for the square container. The walls were attached to a step in the brass bases with a silicone rubber adhesive. The diameters of the fluid layers in the containers were then 11.2 mm for the small circular container, 17.5 mm for the medium circular container, 23.8 mm for the large circular container and 10.5 mm for the square container. In each of the four containers was a fluid layer of the same depth; the depth was measured with a micrometer and was accurate to less than 0.025 mm. In order to reduce the consequences of the meniscus of the fluid layer on the onset and the form of the

ν	ρ	α	κ	S	$\mathrm{d}S/\mathrm{d}T$
cm^2/s	$\mathrm{g/cm}^3$	$^\circ\mathrm{C}^{-1}$	cm^2/s	dyne/cm	dyne/cm °C
1	0.968	0.00096	0.001095	13.96	−0.050

TABLE 1. Properties of the silicone oil at 25 °C

motion of the fluid, the containers were always filled to the rim of the lateral wall, likewise with an accuracy of order of 0.025 mm. The properties of the fluid are listed in table 1. Flow visualization was achieved by aluminium powder suspended in the fluid.

In order to vary the aspect ratio of the fluid layer, the depth of the fluid had to be varied, and therefore also the height of the lateral wall, if the containers were to be filled to the rim. It was also desirable to maintain, in a first approximation, the depth of the air layer between the fluid surface and the glass lid for the different aspect ratios of the fluid layers because the depth of the air layer is very important for the determination of the temperature differences across the fluid. The temperature difference across the fluid has to be calculated from the temperature difference between the brass bases and the cooling water, and follows from the formula

$$\Delta T = \frac{\Delta T_{\mathrm{bw}}}{\left[1+\dfrac{\lambda_{\mathrm{fl}}}{\lambda_{\mathrm{air}}}\dfrac{\Delta Z_{\mathrm{air}}}{\Delta Z_{\mathrm{fl}}}\left(1+\dfrac{\lambda_{\mathrm{air}}}{\lambda_{\mathrm{gl}}}\dfrac{\Delta Z_{\mathrm{gl}}}{\Delta Z_{\mathrm{air}}}\right)\right]}, \tag{3}$$

where ΔT_{bw} is the measured temperature difference between the cooling water and the brass bottom, λ stands for the thermal conductivity of the particular medium, and ΔZ for the thickness of the various layers. Large air gaps permit a relatively accurate determination of the depth of the air gap, but most of the temperature difference between the glass lid and the brass bottom falls off in the air, and therefore the determination of ΔT across the fluid becomes relatively inaccurate. On the other hand, a very small air gap introduces a relatively large inaccuracy in the determination of the depth of the air, which again causes a large uncertainty in ΔT. The depth of the air was therefore held at around 0.5 mm. That required, in particular with the small aspect ratios, that the thickness of the brass bases had to be changed when the aspect ratio of the fluid layer was changed. Using the described arrangement with the four different containers made it possible to study simultaneously the onset of convection and the planform of motion in three circular containers with different aspect ratios and one square container while exactly the same vertical temperature difference was applied to all of them.

3. The experiments

3.1. *Pattern formation*

We begin with experiments with small aspect ratio. We define the aspect ratio A as the ratio of the width of the fluid layer divided by the depth of the fluid. In circular containers we use for the width the diameter of the fluid layer, which practice differs from the definition of the aspect ratio in Rosenblat *et al.* (1982*a*), they use the radius of the fluid layer instead of the diameter. Using the radius for the determination of the aspect ratio introduces a difference of a factor two in the aspect ratios of circular

and square containers of nearly equal size. In rectangular containers the aspect ratio is traditionally the ratio of the horizontal distance between opposite walls and the depth of the fluid.

Since the diameters of the circular containers in our experiments were given, a small aspect ratio meant in our experiments a comparatively large depth of the fluid, which necessarily makes the Rayleigh number comparatively large, because of the dependence of the Rayleigh number on the third power of the depth. In the smallest circular container with the greatest fluid depth we observed onset of convection and moderately supercritical convection in the form of one circular roll, see figure 1 (*a*). Onset of convection was not a spontaneous event, rather the formation of the roll could be observed over a large interval in the applied vertical temperature difference. This is, in all likelihood, due to the presence of the lateral wall; similar wall effects have occurred in all our previous convection experiments, regardless of whether they deal with surface-tension-driven convection or Rayleigh–Bénard convection. An entire series of premature rolls under an air surface has been described in Koschmieder (1967). Over a wide range of aspect ratios ranging from $A = 1.94$ to $A = 4.3$ only one circular roll appeared. The appearance of the circular roll as the first pattern at $A = 1.94$ differs from the results of the calculations of Rosenblat *et al.* (1982*a*), shown on figure 1 of their paper. For their $a = 1$, which is here $A = 2$, the only unstable pattern is a pattern with one azimuthal nodal line and one radial wavenumber. We note that this result is based on the assumption of zero Rayleigh number, no meniscus and adiabatic slip lateral boundary conditions, as well as zero capillary number, which means an inflexible fluid surface. In our experiments with $A \approx 2$ the Rayleigh number is certainly not negligible, the meniscus is practically non-existent, the lateral boundary cannot practically be made strictly adiabatic, the lateral boundary condition is no-slip, and the fluid surface is flexible. The upper boundary condition in our experiments complies with the insulating ($L = 0$) upper boundary used in theory, our lower boundary will be of uniform temperature, as theory assumes. It appears that strict quantitative agreement between theory and experiment cannot be expected.

Decreasing the fluid depth or increasing the aspect ratio produced a two-cellular pattern in the small container at $A = 5.31$, see figure 1 (*b*). With this aspect ratio the stability curves in figure 1 of Rosenblat *et al.* (1982*a*) overlap practically, but the pattern with four azimuthal wavenumbers seems to be the predicted critical pattern. It will, for this A, be quite difficult to establish agreement between theory and experiment, considering the differences between the ideal assumptions of theory and practical necessities of experiments. With $A = 6.05$ we obtained either two or three cells, and with $A = 6.4$ and 6.59 we always obtained three cells (see figure 1*c*). We have also observed completely regular three-cell patterns in the medium and large size circular container (see figures 3*a*, *b*). With $A = 6.79$ and $A = 7.37$ we found very regular four-cell patterns (figure 1*d*), with $A = 8.62$, we had five-cell patterns (figure 1*e*), and with $A = 8.96$ we had either 5 or 6 cells (figure 1*f*), which appeared with equal probability. Decreasing the fluid depth by only 0.05 mm, which meant at an aspect ratio $A = 9.33$, we arrived at a seven-cell pattern (figure 1*g*), where the cell boundaries were no longer exclusively azimuthal nodal lines. Rather the pattern then consisted of one truly hexagonal centre cell, surrounded by 6 regular boundary cells which had only 5 vertices. On figure 1 (*g*) one can also see the direction of motion in the cells. The fluid is rising in the centre of the hexagonal cell, as well as in the centres of the boundary cells. The fluid sinks along the cell boundaries and along the container wall. The location of the ascending fluid is indicated on the photographs by

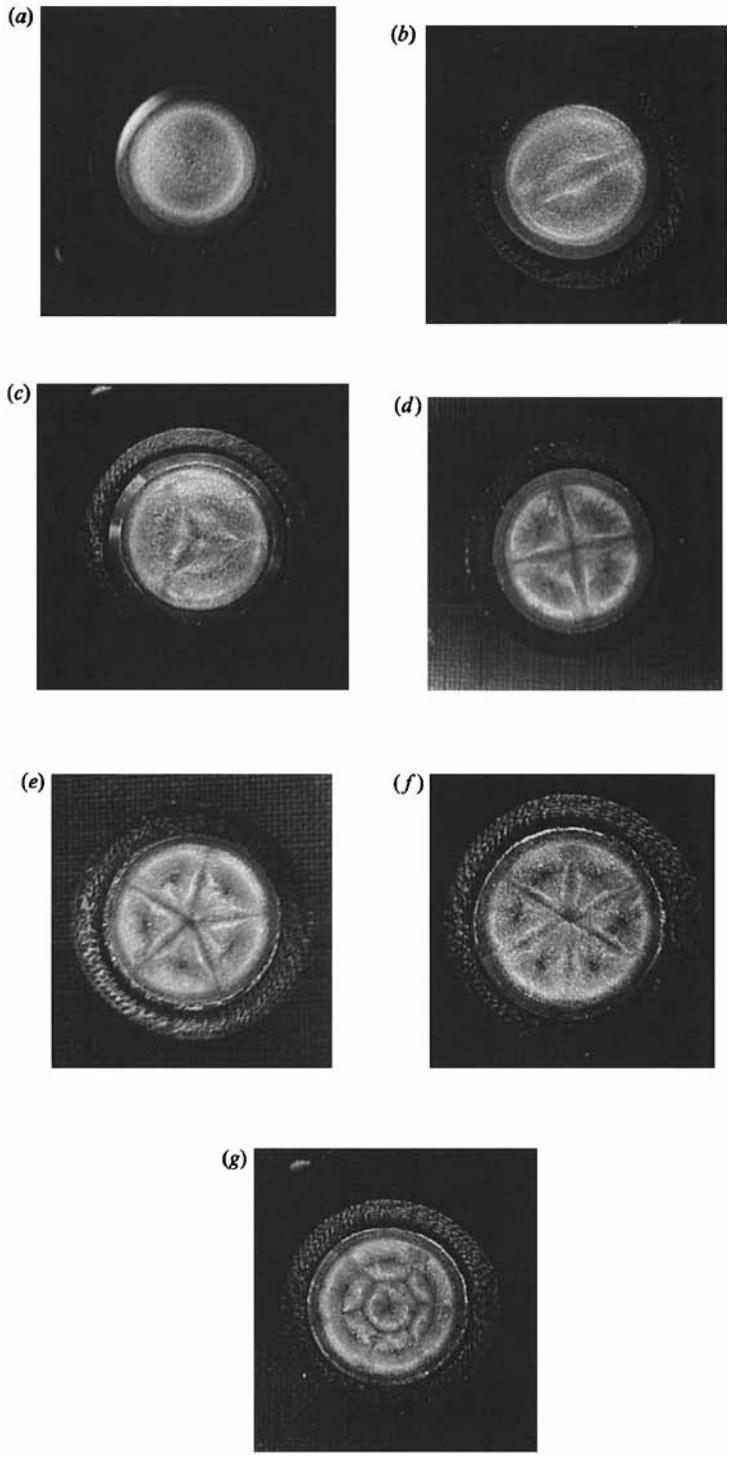

FIGURE 1. The patterns in the small circular container. (*a*) One-cell solution. $M = 330$, $R = 396$, $A = 4.32$. (*b*) Two-cell solution. $Ma = 81$, $R = 65$, $A = 5.31$. (*c*) Three-cell solution. $Ma = 76.5$, $R = 40$, $A = 6.59$. (*d*) Four-cell solution. $Ma = 78$, $R = 38$, $A = 6.79$. (*e*) Five-cell solution. $Ma = 71$, $R = 21$, $A = 8.62$. (*f*) Six-cell solution. $Ma = 74$, $R = 21$, $A = 8.96$. (*g*) Seven-cell solution. $Ma = 67$, $R = 19$, $A = 8.96$.

small (black) lumps of aluminium powder under the centres of the cells. Some aluminium powder settles after a while under the locations of ascending motion. The accumulations of aluminium powder can also be seen in the other patterns shown in figure 1.

Summarizing the results concerning the pattern formation in the small circular container, we find a steady progression of the number of azimuthal nodes in the fluid flow with increased aspect ratio. If, finally, the slices formed by the azimuthal nodes became too elongated, the fluid reverted to the formation of a hexagonal centre cell, surrounded symmetrically by boundary cells.

While the pattern formation in the small circular container seemed to be straightforward, the patterns in the square container are a quite different matter because the fluid has to respond to the delicate question of how to fill a given square area with, e.g. odd numbers of equivalent cells, or likewise with even numbers of cells, exempting those odd or even numbers which are squares, where the fluid obviously has no problems filling a square area with equal cells. We will see that the fluid solves the posed question in a quite unexpected way.

Beginning with an aspect ratio $A = 1.82$, we found one-cellular square cell patterns, as shown in figure 2(*a*). In this figure the fluid rises at the centre of the layer, where the fluid surface is depressed, as was observed visually. The bright ring encircling the centre of the fluid at around half way to the rim indicates the location of maximal elevation of the surface. The fluid sinks along the rim of the container. We note here that the depression of the fluid surface was already noticeable at a seventh of the temperature difference at which the photograph figure 2(*a*) was taken. A picture of such subcritical flow is shown later in figure 4(*b*). The dark crossed lines going away from the centre of the layer were established at twice the temperature difference at which the depression of the fluid surface was first noticed. It may be that the vertical temperature difference was already critical when the dark crossed lines appeared; visual observation is simply inadequate to answer this question, although the motion of the aluminium particles in the fluid was still creeping when the cross at the centre of the layer appeared. Motion of the particles was observed only at around the temperature difference at which figure 2(*a*) was taken. Because of the difficulty in deciding visually the onset of convection, we do not give an apparent critical ΔT for the square pattern. One-cellular square patterns appeared also with the aspect ratios $A = 2.49$ and $A = 4.05$.

At an aspect ratio $A = 4.98$ when in the small circular container the two-cellular pattern was found, a two-cellular pattern was also formed in the square container. The pattern consisted of two triangular cells, as shown with a different aspect ratio in figure 2(*b*). It appears that the fluid prefers this pattern to a solution consisting of two parallel rolls, which is geometrically a possibility, and has been discussed by Rosenblat *et al.* (1982*b*). Flow, as in figure 2(*b*), is rising in the darker areas in the interior of the triangular cells, and sinking along the diagonal of the container and along the rim of the container. The critical condition in this geometry was marked by the formation of the diagonal cell boundary.

At $A = 4.98$ we observed also three-cellular patterns in the square container. Such a pattern is shown in figure 2(*c*); it consists of a square cell in one corner of the container and two wedge-shaped cells filling the rest of the available space. Flow is upwards in the cell centres and downwards at the cell boundaries. This very unusual and unexpected flow was first considered to be an erroneous result, but since it is reproducible and since it is convincingly supported by the form of the six-cellular flow in the square container, the pattern in figure 2(*c*) apparently is the solution

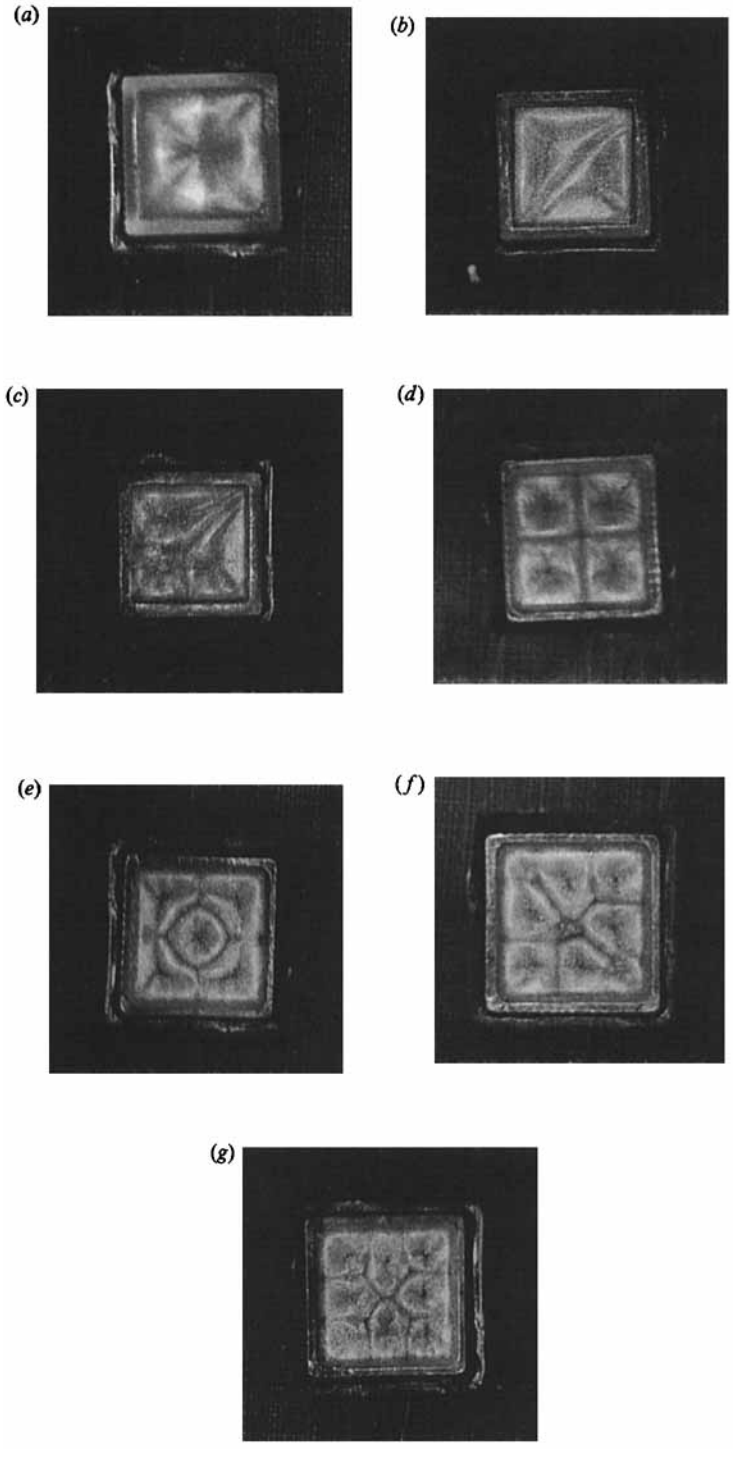

FIGURE 2. The patterns in the square container. (*a*) One-cell solution. $Ma = 380$, $R = 228$, $A = 1.82$. (*b*) Two-cell solution. $Ma = 54$, $R = 33$, $A = 5.68$. (*c*) Three-cell solution. $Ma = 80$, $R = 42$, $A = 6.18$. (*d*) Four-cell solution. $Ma = 78$, $R = 38$, $A = 6.36$. (*e*) Five-cell solution. $Ma = 67$, $R = 19$, $A = 8.4$. (*f*) Six-cell solution. Just critical. $Ma = 72$, $R = 22$, $A = 8.08$. (*g*) Eight-cell solution. $Ma = 63$, $R = 16$, $A = 8.75$.

of the pattern selection mechanism if the aspect ratio provides space for three cells.

At $A = 6.36$ and $A = 6.9$ four regular square cells filled the square container, see figure 2(*d*). This picture was taken in the same experiment and at the same temperature difference as the photograph of the four-cell pattern in the small circular container shown in figure 1(*d*). Note the implication of this pattern for the wavelength of the motions. At $A = 6.36$ the observed critical wavelength in this experiment is $\lambda_c = 3.18$. According to Nield (1964), the critical wavelength for a conducting 'free' surface ($L = \infty$) of surface-tension-driven convection is $\lambda_c = 3.014$, markedly different from the critical wavelength in Rayleigh–Bénard convection, which for rigid–rigid boundaries is $\lambda_c = 2.016$ (Chandrasekhar 1961). In our previous experiments (Koschmieder 1967), we found critical wavelengths ranging from $\lambda_c = 2.70$ to $\lambda_c = 3.12$, for fairly large fluid layers. We note that the theoretical critical wavelengths mentioned refer to infinite fluid layers, and that the presence of the lateral walls can certainly affect the value of λ_c. The requirement that only even numbers of cells fill a container introduces also a principal uncertainty into the determination of λ, which is $\Delta\lambda = \pm\lambda/2N$, where N is the number of pairs of cells in the layer. $\Delta\lambda$ is 0.795 in the case $A = 6.36$.

At $A = 8.08$ the square container exhibited either five or six cells. In the five-cell solution the innermost cell was a square cell (figure 2*e*), whose lateral boundaries were not parallel to the rim of the square container. The rest of the available space was filled with four boundary cells which had five vertices each. This pattern is fairly similar to the seven-cell solution in the circular container (figure 1*g*); both photographs were taken in the same experiment at the same temperature difference. The six-cell pattern in the square container (figure 2*f*) consists of two square cells in opposite corners of the container; the rest of the space is filled with four wedge-shaped cells which we have already encountered in the three-cell pattern (figure 2*c*). The six-cell pattern seems to be a doubled three-cell pattern.

An easy way for the fluid to fill the square container with equal cells would have been the nine square-cell pattern. With $A = 8.75$ we did not, however, obtain nine square cells, but rather an eight-cell solution, consisting of four square cells in the corners of the container and four pentagonal cells whose tips met in the centre of the layer, see figure 2(*g*). Although there seemed to be sufficient space to form a square cell in the centre of the layer, the fluid consistently preferred this eight-cellular pattern. We assume that a nine-cellular square pattern will eventually appear with larger aspect ratios, which we could not realize because the critical temperature differences would then have exceeded safe operating conditions in our apparatus ($\Delta T \approx 40$ °C).

Looking now at the flows in the larger circular containers when the fluid was relatively deep, we found patterns we have already described in figure 1(*a–g*). As examples we show in figures 3(*a*) and 3(*b*) the three-cellular pattern as it appeared in the medium and large circular containers. The aspect ratios in these two cases were $A = 8.29$ and $A = 5.64$. The aspect ratio of the three-cellular pattern in the medium container was unusually large, at the same A we have also observed four-cellular patterns in this container. Note however that $A = 8.29$ corresponds to the upper end of A for the three-cellular pattern permitted by the principal uncertainty of the wavelength for three-cellular flow in bounded containers. In this case $\Delta\lambda/\lambda = \pm 0.30$. Because of the magnitude of the principal uncertainty of the wavelength a three-cellular pattern at $A = 8.29$ is compatible with the three-cellular pattern we have found in the small container at $A = 6.4$ (figure 1*c*). The figures 3(*a*) and 3(*b*) together

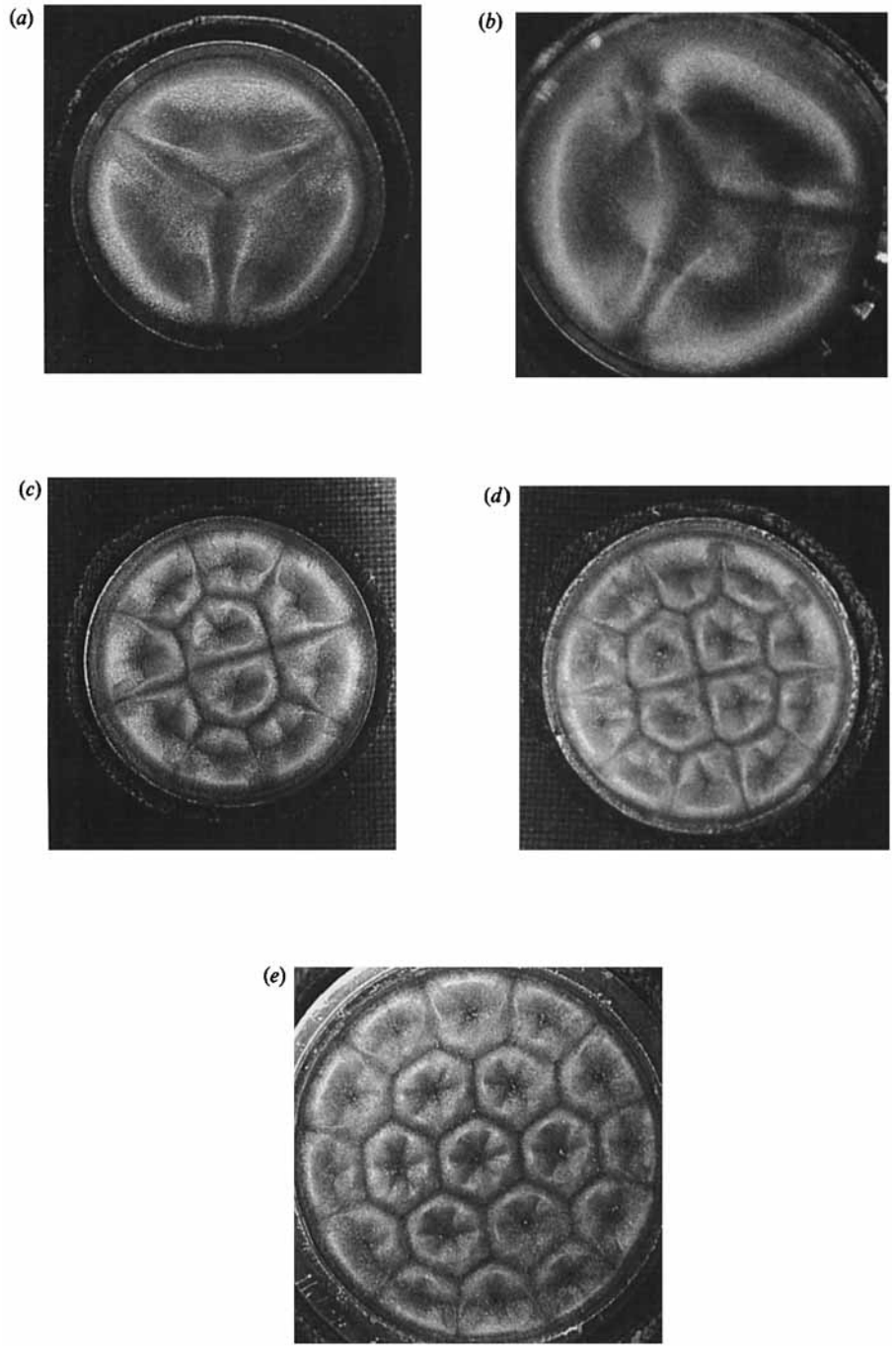

FIGURE 3. Patterns in the medium and large circular container. (*a*) Three-cell solution in the medium container. $Ma = 74$, $R = 59$, $A = 8.29$. The fluid rises in the centres of the three cells and sinks along the wall and the three nodal lines. (*b*) Three-cell solution in the large container. $Ma = 109$, $R = 352$, $A = 5.64$. (*c*). The 2–8 cell solution in the medium container. $Ma = 69$, $R = 33$, $A = 10.8$. The fluid is 1.62 mm deep, the inner diameter of the container is 17.5 mm. (*d*) The 4–10-cell solution in the medium container. $Ma = 75$, $R = 23$, $A = 13.46$. The fluid is 1.30 mm deep. (*e*) The 1–6–12 solution in the large container. $Ma = 88$, $R = 27$, $A = 18.31$. The fluid is 1.30 mm deep, the inner diameter of the container is 23.8 mm.

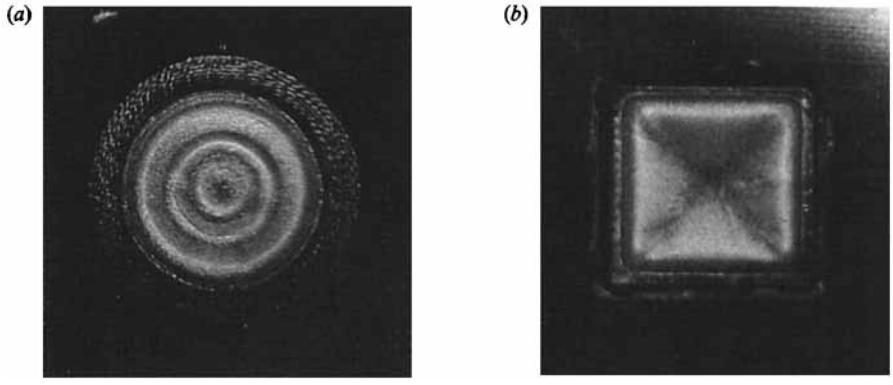

FIGURE 4. (*a*) Subcritical rolls in the small circular container. $Ma = 53$, $R = 14$, $A = 9.33$. (*b*) Subcritical flow in the square container. $Ma = 24$, $R = 7.4$, $A = 8.08$.

with figure 1(*c*) show that the same patterns appear in all three circular containers, if only the fluid depth is chosen correctly so that the aspect ratios are compatible.

For aspect ratios larger than 9.3, at which in the small circular container the seven-cell solution (figure 1*a*) appeared, we found patterns with more than one cell at the centre of the layer, an example of a 2–8 pattern is shown in figure 3(*c*). There were also 3–9 patterns and 4–10 patterns, see figure 3(*d*). In the largest circular container with thin fluid layers, cells arranged in three concentric rings appeared. We want to show only the first such pattern, the 1–6–12 cell form (figure 2*e*). Decreasing the fluid depth further created a multiplicity of solutions which emphasize the hexagonal cell form. This could not be pursued further.

Finally, we want to discuss the subcritical motions which occurred in all containers and accompanied the formation of all patterns. In the circular containers the subcritical motions consisted of circular concentric rolls; an example of such a flow is shown in figure 4(*a*). Such subcritical rolls appear to be the same motions that we have observed earlier (Koschmieder 1967), where we observed up to fifteen concentric rolls under an air surface. Note that the fluid is far from the critical condition for Rayleigh–Bénard convection with a free upper surface. There was, in the 1967 experiment, as well as in the present experiments, very little horizontal non-uniformity of the temperature field. The lateral wall in both experiments is, of course, not perfectly adiabatic; no lateral wall is. Subcritical motions appeared likewise in the square container, already at very low temperature differences, in the form of the diagonal cross shown in figure 4(*b*). The flow indicated by the dark cross is creeping; actual motion of the particles in the fluid could never be seen.

3.2. *The critical condition*

The critical condition of the fluid in the containers was determined visually. It was indicated by the completion of the pattern formation. The patterns do not form spontaneously over the entire layer, but form at the wall and progress towards the centre of the layer. The decision that the formation of a pattern is completed is, of course, somewhat subjective and accompanied by a fairly large uncertainty in ΔT which can easily be 10% and in some cases, such as the one-cellular patterns, may be much more than 10%. The objective way to determine the onset of convection is through heat transfer measurements. We have tried those with a method similar to the method employed in the heat transfer measurements of Koschmieder & Pallas

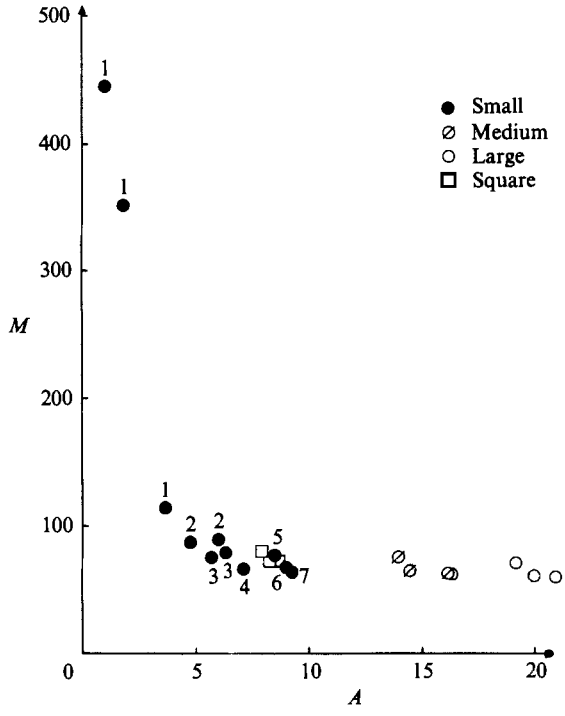

FIGURE 5. The Marangoni numbers at the onset of convection in the different containers and with different aspect ratios. The numbers at the points of the small container indicate the numbers of cells.

(1974). As it turned out, the amount of heat transferred by the fluid in these small containers is so small that the voltage created by the heat sensor is too small in comparison with the outside electrical noise.

The Marangoni numbers determined from the temperature differences at which the patterns established are plotted in figure 5 as a function of the aspect ratio for all containers. While for $A \geqslant 5$ the contribution of the Rayleigh number on the onset of convection is practically negligible, this is not so for $A < 5$. Besides, at the small values of A the uncertainty of the determination of the critical condition becomes very large; the one-cellular pattern in the circular container exists almost from the beginning of heating. One has to use the appearance of visible motion as the criterion for the critical condition in that case. These problems are even worse with the square container; we did not, therefore, determine the critical condition in small-aspect-ratio experiments with the square container. At the small aspect ratios plotted on figure 5, our observations can only be used as a qualitative indication that the critical Maragoni number increases significantly above the value of Ma_c for infinite fluid layers, as was found by Rosenblat *et al.* (1982*a*).

For aspect ratios $A > 5$, the critical Marangoni numbers approach steadily a value $Ma_c \approx 60$. This value is below the expected critical Marangoni number $Ma_c = 79.5$ for infinite fluid layers. There may be two reasons for this discrepancy. There is an experimental uncertainty of about 15% in the determination of the Marangoni number because of the uncertainty of the material constants of the fluid and the uncertainty in the value of the temperature difference. The value of dS/dT is not known with an accuracy better than 5%, and the observed critical temperature differences have a statistical uncertainty of $\pm 3\%$ when $A > 5$. The viscosity as well

as the thermal diffusivity of the fluid is not known with an accuracy better than $\pm 1\%$ either. The applied temperature difference, calculated with equation (3), is uncertain by up to 5%. It may also be that the critical Marangoni number determined theoretically does not apply strictly to our experiments, because of assumptions in the theory which we do not fulfil. We do not mean in this case the consequences of the presence of gravity, which have been calculated by Nield (1964). For the largest containers used in our experiments, the Rayleigh numbers at onset of convection are so small that they cannot explain the change from Ma_c (theor) to Ma_c (exp). One can argue that small horizontal temperature gradients present in the fluid may cause an onset of convection at smaller Marangoni numbers. We note, however, that the critical Marangoni numbers which we found with the same oil in experiments with aspect ratios ranging from $A = 75$ to $A = 188$ were also low, ranging from $Ma_c = 61$ to $Ma_c = 48$ (Koschmieder & Biggerstaff 1986). The fact that we found critical Marangoni numbers of order 60 in the experiments with very large aspect ratios practically eliminates horizontal temperature gradients as the source of the low-value critical Marangoni numbers in our experiments with the small containers. Therefore, we cannot give an explanation for the deviation of the observed value of Ma_c with the largest aspect ratios we used from the theoretical value of Ma_c for an infinite fluid layer.

4. Conclusions

In our experiments studying surface-tension-driven convection in small circular containers we observed a steady increase of the number of azimuthal nodes or cell boundaries from zero on, when we decreased the depth of the fluid layer. Doing so we used always one and the same circular container and arranged that the fluid always filled the container to the rim, and that the thickness of the thin layer of air on top of the fluid remained about the same. Only after the fluid had formed the six-cell pattern with exclusively azimuthal boundaries did, after further decrease of the fluid depth, a pattern appear with a radial node, making space for a hexagonal centre cell surrounded by six boundary cells which were separated by azimuthal nodal lines. Although the order of appearance of the patterns may be different from the order of appearance predicted by Rosenblat *et al.* (1982*a*), it appears that the form of the patterns we observed corresponds to the theoretical expectations. The order of appearance of the patterns in our experiments may be influenced by the lateral boundary conditions and by buoyancy effects. Rosenblat *et al.* use highly simplified lateral boundary conditions. In the corresponding Rayleigh–Bénard convection problem simplified lateral boundary conditions, as studied by Rosenblat (1982), and no-slip boundary conditions, as studied by Charlson & Sani (1971), give different sequences of modal transitions.

The form of the patterns we observed in the square container was a surprise; it does not seem that, for example, the appearance of two triangular cells in the square container was anticipated. Even more so with the form of the three-cell and the six-cell solution in the square container. On the other hand, in the one-cell and the four-cell cases the fluid formed square cells in the interior of the container, as could be expected. As far as the order of appearance of the different patterns was concerned, the number of cells increased steadily with decreased fluid depth in one and the same container, just as it was with the circular container, employing the same precautions as with the circular container. A comparison of our results with the theoretical results of Rosenblat *et al.* (1982*b*) does not seem to be appropriate, because they consider

rectangular containers, of which the square planform is only a very degenerated special case. It would be very instructive to know also the form of the pattern in either square or rectangular containers of small aspect ratio in buoyancy-driven Rayleigh–Bénard convection. A systematic experimental investigation of such flows has, to our knowledge, not yet been made. The consequences of either rigid or slip lateral boundaries for surface-tension-driven convection in rectangular containers have been studied by Dijkstra & van de Vooren (1989). The bifurcations occurring in a two-dimensional rectangular cavity of aspect ratio 2, in either surface-tension or buoyancy-driven flow, have been studied by Winters, Plesser & Cliffe (1988).

Concerning the onset of convection as a function of the aspect ratio of the layer, our measurements confirm in a qualitative way the strong increase of the critical Marangoni number when the aspect ratio decreases to small values of A, as has been predicted by Rosenblat *et al.* (1982*a*).

We thank Mr J. D. Campbell for help with the experiments. Support of this work through the National Aeronautics and Space Agency is gratefully acknowledged.

REFERENCES

BÉNARD, H. 1900 *Rev. Gen. Sci. Pure Appl.* **1**, 1261–1271, 1309–1328.

CHANDRASEKHAR, S. 1961 *Hydrodynamic and Hydromagnetic Stability.* Oxford University Press.

CHARLSON, G. S. & SANI, R. L. 1970 *Intl J. Heat Mass Transfer* **13**, 1479–1496.

CHARLSON, G. S. & SANI, R. L. 1971 *Intl J. Heat Mass Transfer* **14**, 2157–2160.

DAVIS, S. H. 1967 *J. Fluid Mech.* **30**, 465–478.

DIJKSTRA, H. A. & VAN DE VOOREN, A. I. 1989 *Numer. Heat Transfer* **16**, 59–75.

KOSCHMIEDER, E. L. 1967 *J. Fluid Mech.* **30**, 9–15.

KOSCHMIEDER, E. L. & BIGGERSTAFF, M. I. 1986 *J. Fluid Mech.* **167**, 49–64.

KOSCHMIEDER, E. L. & PALLAS, S. G. 1974 *Intl J. Heat Mass Transfer* **22**, 535–546.

NIELD, D. A. 1964 *J. Fluid Mech.* **19**, 341–352.

PEARSON, J. K. A. 1958 *J. Fluid Mech.* **4**, 489–500.

ROSENBLAT, S. 1982 *J. Fluid Mech.* **122**, 395–410.

ROSENBLAT, S., DAVIS, S. H. & HOMSY, G. M. 1982*a* *J. Fluid Mech.* **120**, 91–122.

ROSENBLAT, S., HOMSY, G. M. & DAVIS, S. H. 1982*b* *J. Fluid Mech.* **120**, 123–138.

WINTERS, K. H., PLESSER, TH. & CLIFFE, K. A. 1988 *Physica* D **29**, 387–401.